Molecular Occupancy of Nanodot Arrays

Haogang Cai[1], Haguy Wolfenson[2], David Depoil[3], Michael L. Dustin[3], Michael P. Sheetz[2], and Shalom J. Wind[4,*]

[1]Dept. of Mechanical Engineering, [2]Dept. of Biological Sciences, [4]Dept. of Applied Physics and Applied Mathematics, Columbia University, New York 10027, USA

[3]The Kennedy Institute of Rheumatology, University of Oxford, Oxford, UK OX3 7FY, UK

SUPPLEMENTARY INFORMATION

1. **Fabrication and functionalization**
2. **Molecular model and quenching effect**
3. **Optimal packing problem**
4. **ROI selection and spatial effect correction**
5. **T-cell stimulation by single-molecule nanoarrays**

1. Fabrication and functionalization

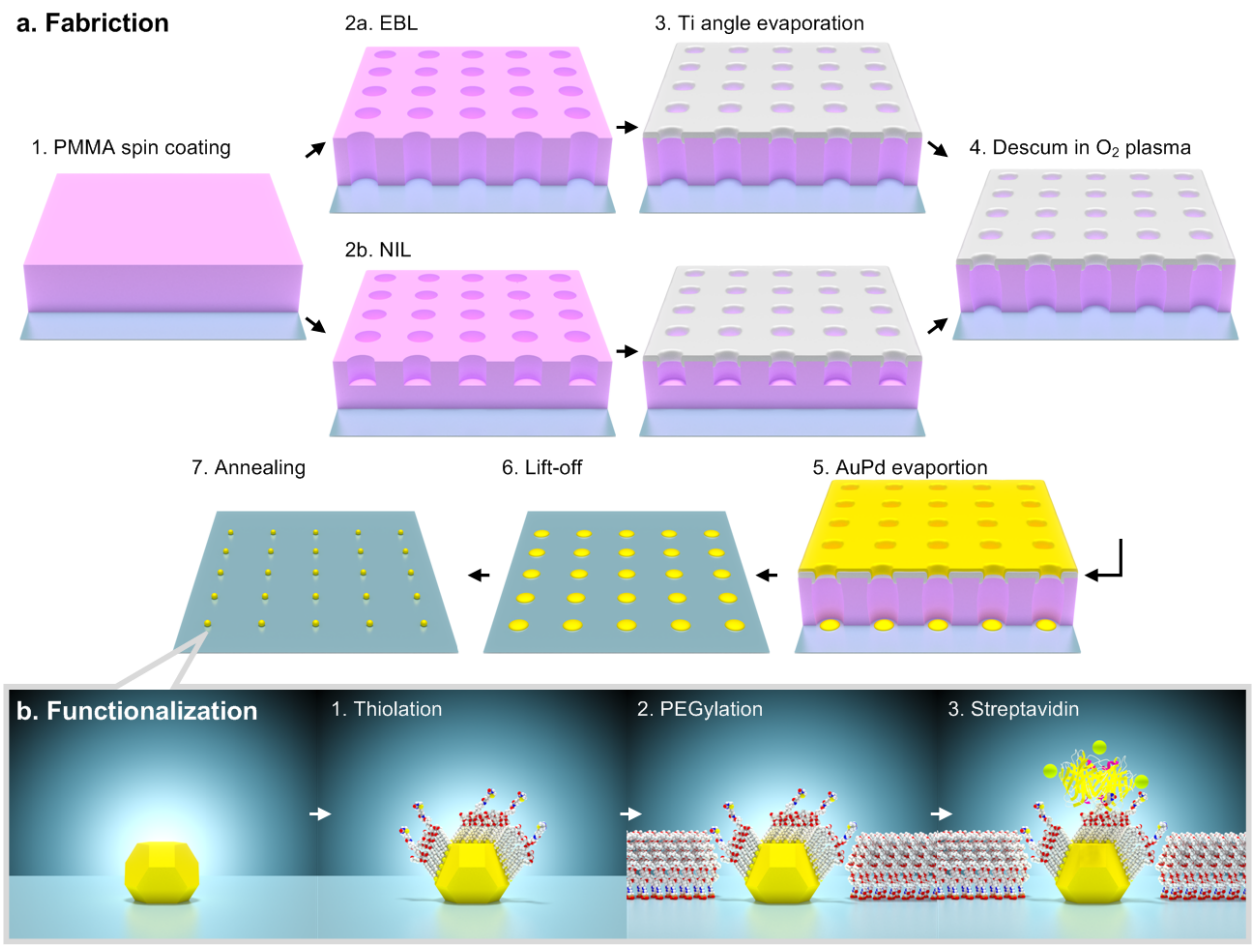

Figure S1. (a) Fabrication and (b) functionalization of AuPd nanodot arrays.

Whereas Au is the most commonly used material for bio-conjugated nanoparticles, exploiting the covalent thiolate linkage to various terminal groups for further functionalization,[1] an AuPd alloy (60/40) was used in this work for the following reasons. First of all, stable self-assembled monolayers (SAMs) with thiol end groups form on AuPd[2] as well as on Pd.[3] Secondly, AuPd is more compatible with our self-aligned nanodot fabrication scheme (Fig. S1a) due to its smaller grain size than Au, which allows it to agglomerate into a single particle at each site. Additionally, as a poor plasmonic metal, Pd particles below 10 nm have no surface plasmon resonance (SPR) in the wavelength range between 300 and 1500 nm.[4] Attenuation of the SPR was found in AuPd bimetallic nanoparticles, from core-shell structures[5, 6] to alloys with various shapes.[7-10] As a result, AuPd nanodots should produce less fluorescence quenching than Au.

2. Molecular model and quenching effect

The molecular model in this study was developed based on the PDB files of alkylthiol and streptavidin-biotin system,[11-14] and visualized by a 3D computer graphics software Blender with ePMV plugin.[15] The morphology of a gold nanoparticle (AuNP) is affected by a variety of factors including size and temperature. Because the gold nanodot was created by top-down lithography instead of synthesis, its shape is more likely thermodynamically preferred truncated octahedron[16] than icosahedron due to growth kinetics.[17] Also, the thermal annealing for the dot size of our interest (≥ 5 nm) should cause only slight modification on (111) surface area of the truncated octahedron, rather than shape transformation.[16, 18] The alkylthiol SAM on a AuNP is quite different from the well-known $(\sqrt{3}\times\sqrt{3})$R30° structure on the (111) bulk surface.[12, 19] Instead, molecular dynamics simulation showed a highly asymmetric arrangement in aqueous solution at room temperature.[20, 21] The exact morphology and SAM distribution of an AuPd nanodot are unknown, but the spatial distribution of primary amines (where fluorophores are bound) can be approximated by this model based on a AuNP.

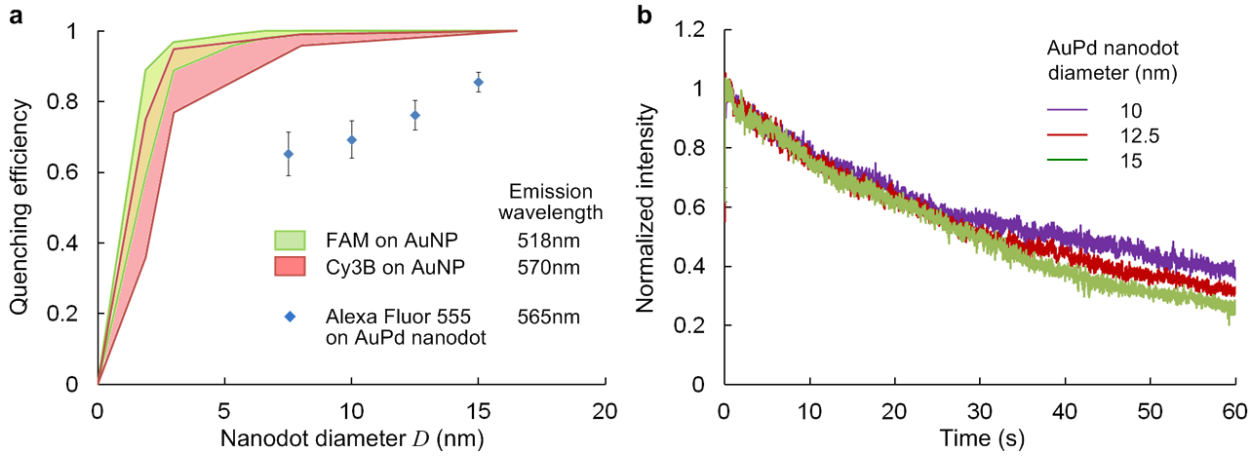

Figure S2. (a) Quenching efficiency *vs.* nanodot diameter. Separation distance in the range of 4.3 - 6.6 nm (data for AuNP from ref [22]). (b) Average bleaching curves for various nanodot size.

For various nanodot size in the given distance range, there is less quenching for AuPd nanodots than for AuNPs[22] (Fig. S2a), because the SPR is attenuated in the AuPd alloy. This aids the bleaching measurements even if the fluorophore emission spectrum (Alexa Fluor 555, almost identical to Cy3) is close to the resonance wavelength of Au (~ 520 nm by Mie theory[23]). The

average bleaching rate also shows dependence on the nanodot size (Fig. S2b). Despite bleaching, the fluorescence was kept over 90% in the first 1 s of exposure, which is used as the initial intensity.

Overall, the quenching effect complicates the measurement, but also provides potential applications. For example, with a spacer of fixed distance, such as DNA instead of streptavidin, this platform can also serve as an alternative for zero mode waveguides (ZMW) to determine the size and distance dependence of quantum yield of single molecules close to metallic nanodots.[24] After calibration of various distances, it can be used as a single-molecule mechanical tension sensor for transmembrane receptors, similar to the single-molecule fluorescence resonance energy transfer (smFRET) technique,[25, 26] but with controlled geometric arrangement.

3. Optimal packing problem

The dependence of molecular occupancy on nanodot size can be interpreted as "the optimal packing of circles on a sphere",[27] sometimes known as the Tammes problem, a specialization of Thomson problem. Considering the protein-repellent layer, it is further simplified as "the packing of circles on a hemisphere"[28] for the dot size of interest. It is assumed that the circles are arranged along concentric circles on the hemisphere and not allowed to cross the boundary. Based on numerical solutions, the elevation, azimuth angles determine the location of each circle, while the viewing angle η determines the circle size, as listed in Table 1.

Table 1. Optimal packing number of circles on a hemisphere

p	η	$\sin \eta = d/D$
1	90	1
2	45	0.707107
3	40.9	0.654741
4	35.3	0.577858
5	30.5	0.507538
6	30	0.5
7	26.6	0.447759
8	23.5	0.398749
9	22.5	0.382683
10	21.6	0.368125

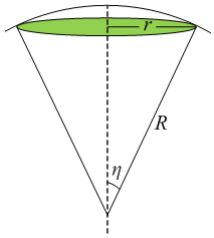

4. ROI selection and spatial effect correction

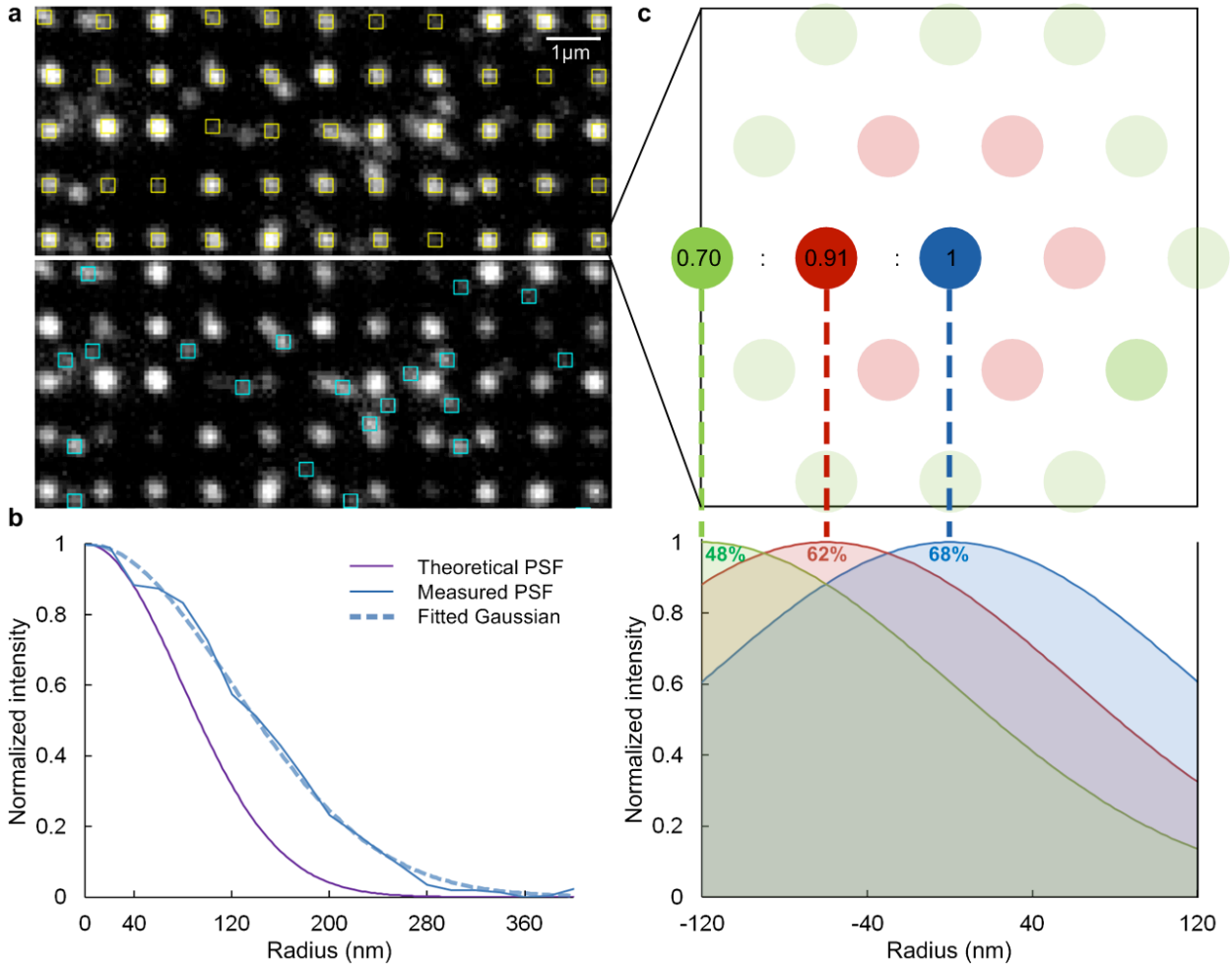

Figure S3. (a) Nanoarray fluorescence image and separate ROIs (yellow: signals of nanodot array, cyan: noises of nonspecific bound fluorophores). (b) Theoretical and measured PSFs. (c) A close-up of a 3×3 pixel ROI and the nanodot spatial effect on intensity. (Scale: 80nm/pixel)

An array of single dots was used to measure the point-spread function (PSF) by FIJI using the "Mosaic" plug-in.[29] Its fitted Gaussian has a radius (standard deviation) of 1.5 pixels (120 nm) (Fig. S3b). A 1D approximation indicates that ~ 68% of the intensity is within a 3×3 pixel region, which is chosen as the region of interest (ROI) for the measurement of both initial intensity and bleaching step size. It not only ensures a high signal-to-background ratio (SBR), but also considers the spatial fluctuation of intensity profiles during bleaching.

The nanodots in each cluster are not in the same position, but in a hexagonal arrangement with 60 nm spacing. Hence, the individual positions have a spatial effect on the total intensity of a cluster. The intensity in the given ROI includes 68% of the central nanodot, 62% of the nanodot

60 nm away, and only 47% of the nanodot 120 nm away (Fig. S3c). The resulted cluster intensity relative to the intensity of all the fluorescence in the center is listed in Table 2, based on a 1D approximation. Molecular occupancy correction coefficients for various cluster size are calculated relative to a heptamer, which the bleaching step size measurement was based on.

Table 2. Correction coefficients for various cluster size.

Cluster size *c*	1	2	3	4	5	6	7	10	14	19
Relative intensity in a 3×3 pixel ROI	1.0000	0.9575	0.9433	0.9362	0.9320	0.9292	0.9271	0.8587	0.8131	0.7831
Correlation coefficient	0.9271	0.9683	0.9828	0.9903	0.9948	0.9978	1.0000	1.0797	1.1402	1.1839

5. T-cell stimulation by single-molecule nanoarrays

Similarly to streptavidin-555, the bleaching step size histogram for UCHT1 Fab'-568 on 7.5 nm AuPd nanodot was fitted to a mixed Gaussian distribution (Fig. S4a). The second peak represents simultaneous bleaching events, which counts less than streptavidin, because the total number of fluorophores is much less. The F/P ratio of streptavidin was 3, while that of Fab' was only 0.45, in order to maintain the best function. This bleaching step size distribution was then used as a single Gaussian to estimate the fluorophore occupancy by multiple Gaussian fit of intensity distribution (Fig. S4b and inset). On average, there were 3 ± 1.8 fluorophores per heptamer, *i.e.*, 0.98 ± 0.58 Fab' per nanodot, close to a single molecule occupancy.

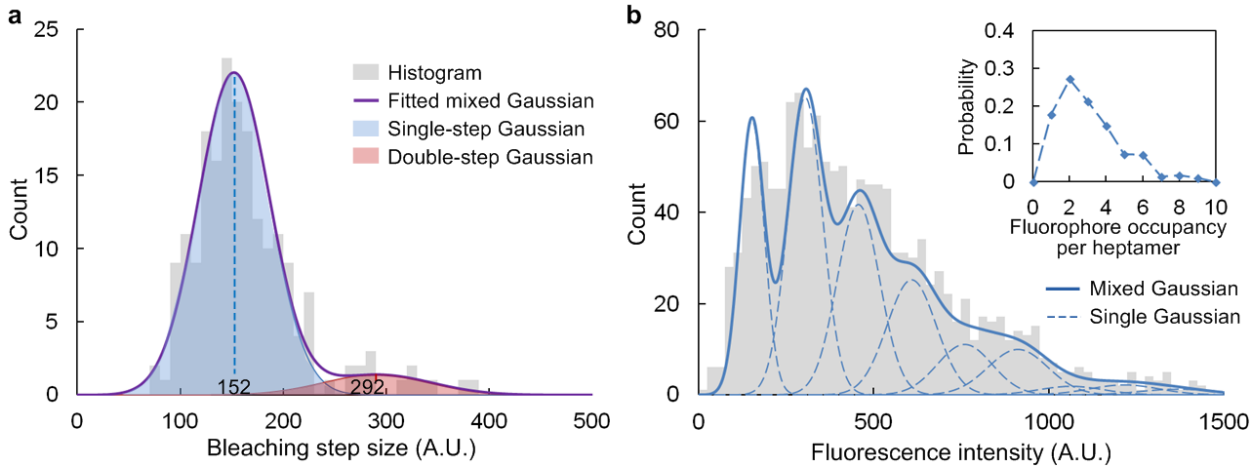

Figure S4. Histograms of UCHT1 Fab'-568 (D = 7.5nm, x = 50%): (a) bleaching step size and (b) fluorescence intensity and fluorophore occupancy per heptamer.

The molecular occupancy in the work by Deeg *et al.*[30] was estimated by the intensity of a 110 μm^2 hexagonal array (*e.g.*, including 35283 dots when the spacing is 60 nm) and the average intensity on a single spot. The latter was achieved by a low functionalization concentration and then assumed to be the single molecule intensity. It was a small divisor compared with the large area intensity, which could cause a large measurement error. The background variation among different samples also contributed to the large variation of molecular occupancy. A few samples were only partially functionalized, and the rest ranged from single to six molecules per dot. The estimated occupancy (not single-molecule) could be used to correct the global density threshold, but is not applicable for local spacing or stoichiometry effect.

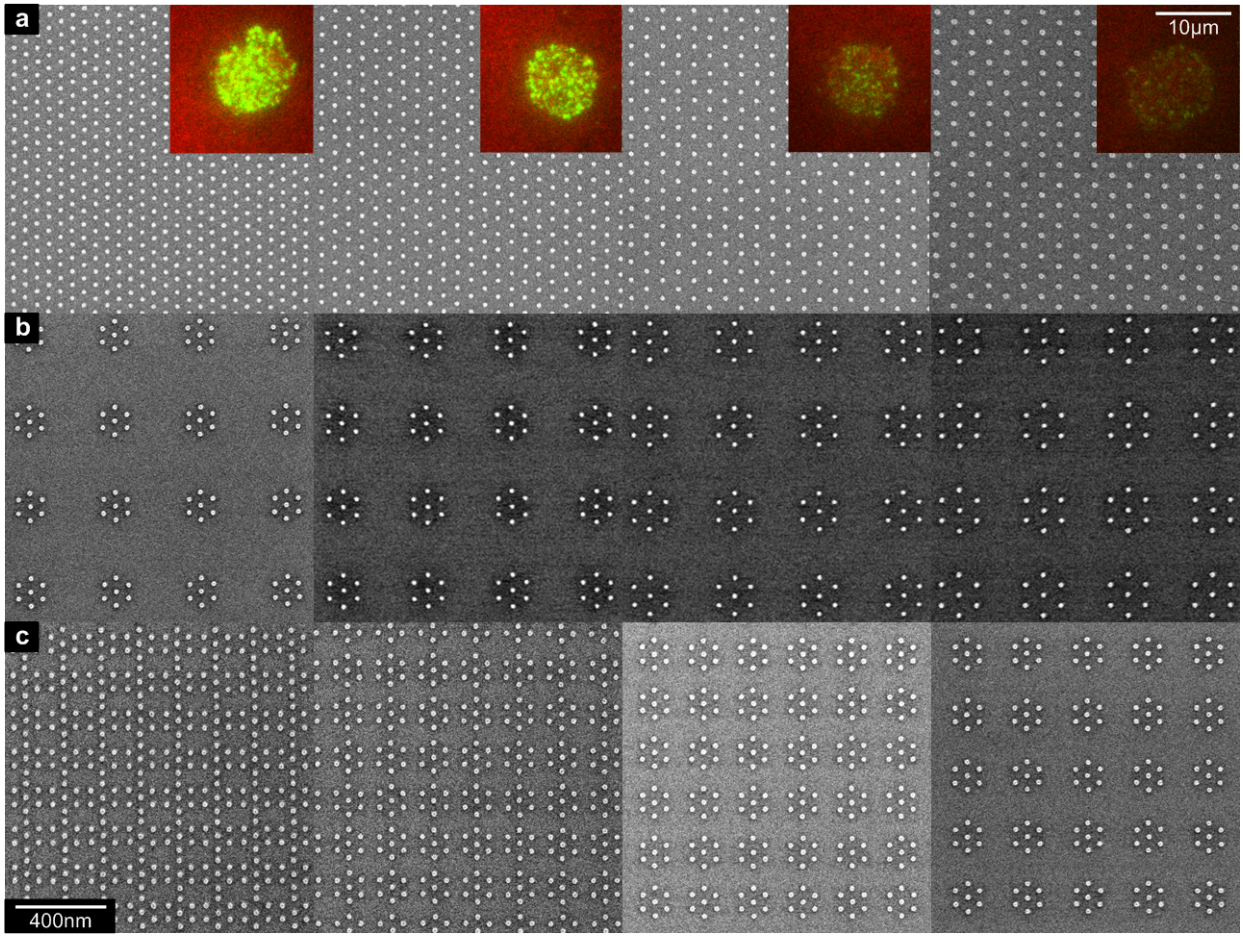

Figure S5. Various patterns on a same NIL mold (whose feature size is larger than the final nanodot size, therefore showing a more clear pattern) for T-cell assays: (a) hexagonal arrays with spacing 60 - 90 nm (insets are corresponding cell assay fluorescence images. green: pY-488, red: UCHT1 Fab'-568), (b) 50 /μm^2 heptamer arrays with inter-dot spacing 60 - 90 nm, (c) 60 nm heptamer arrays with dot density 100 - 250 /μm^2.

Single-molecule occupancy is a basic assumption in cellular studies using nanodot arrays,[30-39] but the tolerance depends on the dimension of the transmembrane receptors, which bind to ligands immobilized on the nanodots. For small receptors, *e.g.,* the T-cell receptor (TCR, a heterodimer with two ~ 40 - 50 kD chains[40]), single ligand occupancy is critical, while a rough control probably contributes to a great variation in probing the T-cell activation among different platforms, especially for those using the same cell type and similar ligands (Table 3).[30, 33, 36] For large receptors, *e.g.,* integrins (the head is ~ 8 - 12 nm), single-molecular occupancy is assured as long as the nanodot is smaller than the receptor, even if each nanodot presents multiple ligands. Nanoarrays of integrin binding ligand RGD (Arg-Gly-Asp) were used to explore the geometric effect on cell adhesion and spreading. A spatial threshold of ~ 60 nm was obtained in many experiments using either BCML or EBL/NIL (Table 4).[32, 37-39]

Table 3. T-cell activation on nanoarrays of TCR binding sites.

Refer-ence	T-cell type	TCR binding ligand	Activation index	Cell assay	Adhesive or costimulatory molecule	Threshold (transition region)	Linking chemistry	Dot size	Molecular occupancy
Spatz [30]	Mouse $CD4^+$	pMHC	contact area, adhesion %, IL2 secretion	45 min, 24 hr	No	100 - 150 nm (70 /μm^2)*	Histag, Ni-NTA thiol	NA	1.6
Spatz [33]	Human $CD4^+$	aCD3 OKT3	IL2 secretion, proliferation	17 hr, 4 days	aCD28	≥ 150 nm	Histag, Ni-NTA thiol	NA	NA
Dunlop [36]	Human $CD4^+$	aCD3 UCHT1 $F(ab')_2$	pY intensity, cell density	5 min	ICAM-1	34 - 69 nm	Thiol	8 - 17 nm	NA
This work	Human $CD4^+$	aCD3 UCHT1 Fab'	pY intensity	5 min	ICAM-1	100 nm (115 /μm^2)	Biotin, Streptavidin-biotin thiol	7.5 nm	0. 98

* corrected by the molecular occupancy: 70 × (1.6 ± 0.4), *i.e.*, 90 - 140 /μm^2.

Table 4. Cell adhesion and spreading on nanoarrays of integrin binding sites.

References	Cell type	Integrin binding ligand	Adhesion and spreading index	Threshold (transition region)	Linking chemistry	Dot size
Spatz [37-39]	MC3T3-osteoblasts B16-melanocytes REF52-fibroblasts 3T3-fibroblasts	RGD	% of spreading cells	58 - 73nm	Histag, Ni-NTA thiol	< 8 nm
Wind [32]	3T3-fibroblasts	RGD	% of spreading cells	60 - 80 nm	Biotin, Streptavidin-biotin thiol	sub-10 nm

Table 5. List of PDB files used in the molecular 3D model

Molecule	PDB file name	PDB ID
Streptavidin-biotin	Wildtype Core-Streptavidin with Biotin at 1.4A	1MK5 [13]
	PENTADECANE	MYS
Alkylthiol	E-AMINO BIOTINYL CAPROIC ACID	BH7
	POLYETHYLENE GLYCOL (N=34), PEG1500	15P
PEG-silane	ETHYL-TRIMETHYL-SILANE	CEQ

Table 6. Variables list

c	Cluster size, *i.e.*, the number of nanodots per cluster
D	Diameter of nanodot (nm)
d	Diameter of molecule (nm)
h	Photobleaching step size (A. U.)
I	Initial intensity (A. U.)
N	Molecular occupancy
n	Sample size
P	Probability of a distribution
p	Optimal packing number
r	F/P ratio, *i.e.*, the number of fluorophores per molecule
S	Separation distance (nm)
x	Mole fraction of binding ligands

References

1. Love, J. C.; Estroff, L. A.; Kriebel, J. K.; Nuzzo, R. G.; Whitesides, G. M. Self-Assembled Monolayers of Thiolates on Metals as a Form of Nanotechnology. *Chem. Rev.* 2005, 105, 1103-1169.
2. Cherniavskaya, O.; Chen, C. J.; Heller, E.; Sun, E.; Provezano, J.; Kam, L.; Hone, J.; Sheetz, M. P.; Wind, S. J. Fabrication and Surface Chemistry of Nanoscale Bioarrays Designed for the Study of Cytoskeletal Protein Binding Interactions and Their Effect on Cell Motility. *J. Vac. Sci. Technol. B* 2005, 23, 2972.
3. Love, J. C.; Wolfe, D. B.; Haasch, R.; Chabinyc, M. L.; Paul, K. E.; Whitesides, G. M.; Nuzzo, R. G. Formation and Structure of Self-Assembled Monolayers of Alkanethiolates on Palladium. *J. Am. Chem. Soc.* 2003, 125, 2597-2609.

4. Xiong, Y. J.; Chen, J. Y.; Wiley, B.; Xia, Y. N.; Yin, Y. D.; Li, Z. Y. Size-Dependence of Surface Plasmon Resonance and Oxidation for Pd Nanocubes Synthesized *via* a Seed Etching Process. *Nano Lett.* 2005, 5, 1237-1242.
5. Njoki, P. N.; Solomon, L. V.; Wu, W. J.; Alam, R.; Maye, M. M. Attenuating Surface Plasmon Resonance *via* Core/Alloy Architectures. *Chem. Commun.* 2011, 47, 10079-10081.
6. Chiu, C. Y.; Yang, M. Y.; Lin, F. C.; Huang, J. S.; Huang, M. H. Facile Synthesis of Au-Pd Core-Shell Nanocrystals with Systematic Shape Evolution and Tunable Size for Plasmonic Property Examination. *Nanoscale* 2014, 6, 7656-7665.
7. Wu, M. L.; Chen, D. H.; Huang, T. C. Synthesis of Au/Pd Bimetallic Nanoparticles in Reverse Micelles. *Langmuir : the ACS journal of surfaces and colloids* 2001, 17, 3877-3883.
8. Chen, Y. H.; Tseng, Y. H.; Yeh, C. C. Laser-Induced Alloying Au-Pd and Ag-Pd Colloidal Mixtures: The Formation of Dispersed Au/Pd and Ag/Pd Nanoparticles. *J. Mater. Chem.* 2002, 12, 1419-1422.
9. Lee, Y. W.; Kim, N. H.; Lee, K. Y.; Kwon, K.; Kim, M.; Han, S. W. Synthesis and Characterization of Flower-Shaped Porous Au-Pd Alloy Nanoparticles. *J Phys Chem C* 2008, 112, 6717-6722.
10. Lee, Y. W.; Kim, M.; Kim, Y.; Kang, S. W.; Lee, J. H.; Han, S. W. Synthesis and Electrocatalytic Activity of Au-Pd Alloy Nanodendrites for Ethanol Oxidation. *J Phys Chem C* 2010, 114, 7689-7693.
11. Lee, J.; Kim, S. H. Pdb Editor: A User-Friendly Java-Based Protein Data Bank File Editor with a Gui. *Acta Crystallogr D* 2009, 65, 399-402.
12. Latour, R. A.; Rini, C. J. Theoretical Analysis of Adsorption Thermodynamics for Hydrophobic Peptide Residues on Sam Surfaces of Varying Functionality. *Journal of Biomedical Materials Research* 2002, 60, 564-577.
13. Hyre, D. E.; Le Trong, I.; Merritt, E. A.; Eccleston, J. F.; Green, N. M.; Stenkamp, R. E.; Stayton, P. S. Cooperative Hydrogen Bond Interactions in the Streptavidin-Biotin System. *Protein Sci.* 2006, 15, 459-467.
14. Bernstein, F. C.; Koetzle, T. F.; Williams, G. J. B.; Meyer, E. F.; Brice, M. D.; Rodgers, J. R.; Kennard, O.; Shimanouchi, T.; Tasumi, M. Protein Data Bank - Computer-Based Archival File for Macromolecular Structures. *J. Mol. Biol.* 1977, 112, 535-542.
15. Johnson, G. T.; Autin, L.; Goodsell, D. S.; Sanner, M. F.; Olson, A. J. Epmv Embeds Molecular Modeling into Professional Animation Software Environments. *Structure* 2011, 19, 293-303.
16. Barnard, A. S.; Lin, X. M.; Curtiss, L. A. Equilibrium Morphology of Face-Centered Cubic Gold Nanoparticles > 3 nm and the Shape Changes Induced by Temperature. *J. Phys. Chem. B* 2005, 109, 24465-24472.
17. Barnard, A. S.; Chen, Y. Kinetic Modelling of the Shape-Dependent Evolution of Faceted Gold Nanoparticles. *J. Mater. Chem.* 2011, 21, 12239-12245.
18. Kuo, C. L.; Clancy, P. Melting and Freezing Characteristics and Structural Properties of Supported and Unsupported Gold Nanoclusters. *J. Phys. Chem. B* 2005, 109, 13743-13754.
19. Ulman, A.; Eilers, J. E.; Tillman, N. Packing and Molecular-Orientation of Alkanethiol Monolayers on Gold Surfaces. *Langmuir : the ACS journal of surfaces and colloids* 1989, 5, 1147-1152.
20. Lane, J. M. D.; Grest, G. S. Spontaneous Asymmetry of Coated Spherical Nanoparticles in Solution and at Liquid-Vapor Interfaces. *Phys. Rev. Lett.* 2010, 104.
21. Luedtke, W. D.; Landman, U. Structure and Thermodynamics of Self-Assembled Monolayers on Gold Nanocrystallites. *J. Phys. Chem. B* 1998, 102, 6566-6572.
22. Breshike, C. J.; Riskowski, R. A.; Strouse, G. F. Leaving Forster Resonance Energy Transfer Behind: Nanometal Surface Energy Transfer Predicts the Size-Enhanced Energy Coupling between a Metal Nanoparticle and an Emitting Dipole. *J Phys Chem C* 2013, 117, 23942-23949.
23. Hu, M.; Chen, J. Y.; Li, Z. Y.; Au, L.; Hartland, G. V.; Li, X. D.; Marquez, M.; Xia, Y. N. Gold Nanostructures: Engineering Their Plasmonic Properties for Biomedical Applications. *Chem. Soc. Rev.* 2006, 35, 1084-1094.

24. Holzmeister, P.; Pibiri, E.; Schmied, J. J.; Sen, T.; Acuna, G. P.; Tinnefeld, P. Quantum Yield and Excitation Rate of Single Molecules Close to Metallic Nanostructures. *Nat Commun* 2014, 5.
25. Stabley, D. R.; Jurchenko, C.; Marshall, S. S.; Salaita, K. S. Visualizing Mechanical Tension across Membrane Receptors with a Fluorescent Sensor. *Nat. Methods* 2012, 9, 64-U172.
26. Roy, R.; Hohng, S.; Ha, T. A Practical Guide to Single-Molecule FRET. *Nat. Methods* 2008, 5, 507-516.
27. Clare, B. W.; Kepert, D. L. The Optimal Packing of Circles on a Sphere. *J. Math. Chem.* 1991, 6, 325-349.
28. Appelbaum, J.; Weiss, Y. The Packing of Circles on a Hemisphere. *Measurement Science & Technology* 1999, 10, 1015-1019.
29. Sbalzarini, I. F.; Koumoutsakos, P. Feature Point Tracking and Trajectory Analysis for Video Imaging in Cell Biology. *J Struct Biol* 2005, 151, 182-195.
30. Deeg, J.; Axmann, M.; Matic, J.; Liapis, A.; Depoil, D.; Afrose, J.; Curado, S.; Dustin, M. L.; Spatz, J. P. T Cell Activation Is Determined by the Number of Presented Antigens. *Nano Lett* 2013, 13, 5619-26.
31. Cai, H.; Depoil, D.; Palma, M.; Sheetz, M. P.; Dustin, M. L.; Wind, S. J. Bifunctional Nanoarrays for Probing the Immune Response at the Single-Molecule Level. *Journal of vacuum science and technology. B, Nanotechnology & microelectronics : materials, processing, measurement, & phenomena : JVST B* 2013, 31, 6F902.
32. Schvartzman, M.; Palma, M.; Sable, J.; Abramson, J.; Hu, X.; Sheetz, M. P.; Wind, S. J. Nanolithographic Control of the Spatial Organization of Cellular Adhesion Receptors at the Single-Molecule Level. *Nano Lett* 2011, 11, 1306-12.
33. Matic, J.; Deeg, J.; Scheffold, A.; Goldstein, I.; Spatz, J. P. Fine Tuning and Efficient T Cell Activation with Stimulatory Acd3 Nanoarrays. *Nano Lett.* 2013, 13, 5090-5097.
34. Jaehrling, S.; Thelen, K.; Wolfram, T.; Pollerberg, G. E. Nanopatterns Biofunctionalized with Cell Adhesion Molecule DM-GRASP Offered as Cell Substrate: Spacing Determines Attachment and Differentiation of Neurons. *Nano Lett.* 2009, 9, 4115-4121.
35. Ranzinger, J.; Krippner-Heidenreich, A.; Haraszti, T.; Bock, E.; Tepperink, J.; Spatz, J. P.; Scheurich, P. Nanoscale Arrangement of Apoptotic Ligands Reveals a Demand for a Minimal Lateral Distance for Efficient Death Receptor Activation. *Nano Lett.* 2009, 9, 4240-4245.
36. Delcassian, D.; Depoil, D.; Rudnicka, D.; Liu, M. L.; Davis, D. M.; Dustin, M. L.; Dunlop, I. E. Nanoscale Ligand Spacing Influences Receptor Triggering in T Cells and NK Cells. *Nano Lett.* 2013, 13, 5608-5614.
37. Arnold, M.; Cavalcanti-Adam, E. A.; Glass, R.; Blummel, J.; Eck, W.; Kantlehner, M.; Kessler, H.; Spatz, J. P. Activation of Integrin Function by Nanopatterned Adhesive Interfaces. *Chemphyschem* 2004, 5, 383-388.
38. Cavalcanti-Adam, E. A.; Volberg, T.; Micoulet, A.; Kessler, H.; Geiger, B.; Spatz, J. P. Cell Spreading and Focal Adhesion Dynamics Are Regulated by Spacing of Integrin Ligands. *Biophys. J.* 2007, 92, 2964-2974.
39. Huang, J. H.; Grater, S. V.; Corbellinl, F.; Rinck, S.; Bock, E.; Kemkemer, R.; Kessler, H.; Ding, J. D.; Spatz, J. P. Impact of Order and Disorder in Rgd Nanopatterns on Cell Adhesion. *Nano Lett.* 2009, 9, 1111-1116.
40. Weiss, A. Structure and Function of the T-Cell Antigen Receptor. *J. Clin. Invest.* 1990, 86, 1015-1022.